New Advances in Air-Coupled Ultrasonic NDT Using Acoustic Mode Conversion

I. SOLODOV and G. BUSSE, Institute for Polymer Testing and Polymer Science (IKP), Non-destructive Testing (ZFP), University of Stuttgart, Stuttgart, Germany

Abstract. Air-coupled ultrasound is a well-established tool for acoustic NDT and material characterization. Its major shortcoming is concerned with a weak penetration into material due to a severe impedance mismatch at the air-solid interface. A strong rise in acoustic coupling to solids is obtained by using acoustic mode conversion in slanted configurations. In our experiments, a substantial increase of the ultrasound amplitude was observed in various solid materials (metals, wood, concrete, composites) under phase matching conditions for plate and surface acoustic waves. On this basis, fully air-coupled and hybrid air-coupled-optic configurations are developed and applied for non-contact NDT. New opportunities of the mode conversion approach are demonstrated in remote mapping of elastic anisotropy, drying and thickness measurements of paint films, and ultrasonic imaging of defects.

1. Introduction

In recent years, air-coupled ultrasound (ACU) has become a routine inspection technique in non-destructive testing (NDT) of a wide range of materials and components [1]. However, in conventional Normal Transmission Mode (NTM) of ACU-systems, the transmission of ultrasonic energy into solids is extremely inefficient (~10^{-4}) due to the mismatch of acoustic impedances (4-5 orders of magnitude for the majority of materials). The situation is aggravated if the materials, like composites, are laminated, porous or highly dissipative. As a result, conventional NDT with ACU is virtually not applicable to “inconvenient” materials, like plastics, foams, some composites, wood, and cement based materials.

To increase the elastic coupling between air and solids, one can use the idea of spatial resonance. The first option includes thickness resonance which strongly enhances vibration amplitude (and ACU transmission) in plate-like samples. In slanted ACU configurations, the spatial resonance corresponds to constructive interference of the waves along a particular in-plane direction. In thin samples, this causes a resonance generation of plate acoustic waves (PAW) while an efficient excitation of surface acoustic waves (SAW) is expected when the thickness of the specimen is greater than a few wavelengths.

In this paper, several new approaches to non-contact NDT of various materials based on conversion of focused ACU into plate and surface waves are reported. The applications developed include remote imaging of defects, mapping of in-plane elastic anisotropy, drying and thickness measurements of paint coatings.

2. Theoretical background

It is well-known that reflection-transmission of elastic waves at oblique incidence on a solid interface results in producing of new types of waves (mode conversion) [2]. The directions of propagation of the reflected-transmitted waves are determined by Snell`s law while efficiency of the conversion into the new modes can be rather high [3]. In the ACU

configuration, this can be used to increase transmission of ultrasound into solids beyond conventional threshold determined by impedance mismatch.

Such a case was demonstrated [4] for plane acoustic wave transmission through a solid plate separating two elastic media. If the impedance of the surrounding medium (air) is much less than that of the sample, the transmission coefficient displays a singularity, i.e. a total transmission is expected at an optimum angle of incidence (θ_0) providing a phase matching between the incident wave and the plate (Lamb) mode:

$$v_{air} / \sin\theta_0 = v_p \ , \qquad (1)$$

where v_p is the phase velocity of the plate wave.

Physically, this condition corresponds to an efficient excitation of the plate waves by obliquely incident ACU which then re-radiate acoustic energy in air from the rear side of the sample. The results of calculations (based on the matrix approach suggested in [4]) of the ACU transmission as a function of angle of incidence for a PMMA plate are shown in Fig. 1. The two θ_0-peaks correspond to velocities of the symmetrical (s_0) and anti-symmetrical (a_0) zero-order modes calculated from (1). The higher-order modes are not excited [5] because their acoustic displacements are localised in the interior of the sample and the field is "locked" inside the sample thereby preventing access from/to the surface.

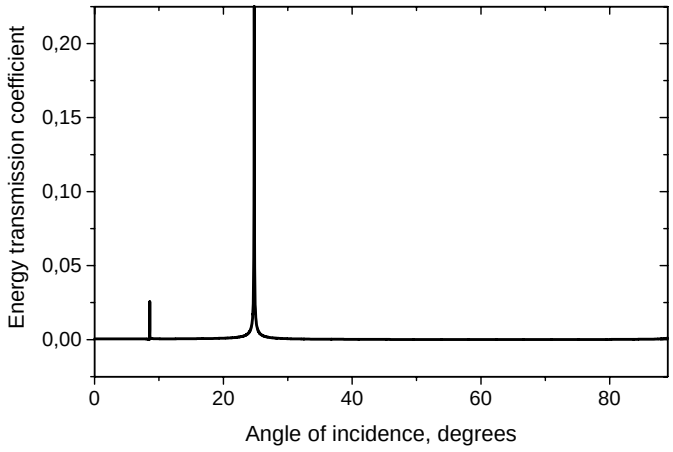

Figure 1. Transmission coefficient as a function of angle of incidence for a 0.5 mm PMMA plate in air (frequency $f = 450\ kHz$).

The efficiency of conversion also depends on the polarization of the waves excited: ACU coupling is provided only to the out-of-plane components of displacement. According to the calculations [6], the out-of-plane displacement dominates in the zero-order anti-symmetric modes (a_0) in thin plates. For this reason, the conversion efficiency into such flexural waves is usually much higher than that for any other plate wave mode. Despite the higher efficiency, the flexural wave excitation in very thin plates (films) may be not possible due to specific dispersion properties: for $k_t D \to 0$ (k_t is the wave number of shear wave) the flexural wave velocity goes to zero and $\sin\theta_0 > 1$ in (1). To avoid this, one should keep the ultrasonic frequency high enough to provide $v_p > v_{air}$.

For thicker plates, the excitation efficiencies are comparable for both of the zero-order modes (a_0 and s_0) while their velocities approach to the velocity of SAW (or Rayleigh wave). The acoustic field formed by these modes is shown in Fig. 2 and demonstrates that acoustic displacements are concentrated near each of the free surfaces of the plate. However, the anti-phase interference of the in-plane (U) and out-of-plane (W) components of both modes at a rear surface (0>x>-D/2, Fig. 2) provides an exclusive

single-surface localization and turn the acoustic field into a Rayleigh wave propagating along the free surface of the plate where the wave is excited. The ACU is not transmitted through the specimen anymore but can be detected in a single-sided configuration. The optimal angles of the ACU conversion into SAW are given by (1) where $v_p \to v_{SAW}$.

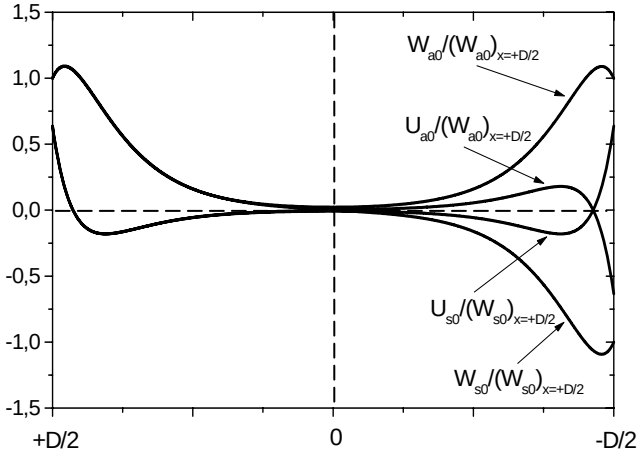

Figure 2. Depth distributions of normalized displacements of zero-order modes in PMMA plate at $k_t D = 30$.

The surface waves are also polarized mainly out-of-plane (Fig. 2) so that one would expect their strong coupling to ACU. Unlike (1), which is derived for a plane wave ACU, in a realistic case of a finite aperture incident beam, the mode conversion will also take place at θ different from θ_0. In this case, the angular dependence of the conversion efficiency is derived by the k-space Fourier transform of the surface excitation function:

$$F(k) = b \sin[(k_{air} \sin\theta - k)b/2]/[(k_{air} \sin\theta - k)b/2]. \quad (2)$$

The results of calculations of the ACU-SAW conversion from (2) ($k = k_{SAW}$) in PMMA for 400 kHz-ACU are shown in Fig. 3. The higher conversion efficiency is observed for greater b at the expense of a narrower angular range of excitation. In the limit of $b \to \infty$, (3) yields a δ-function type dependence and a single angle of excitation θ_0 given by (1).

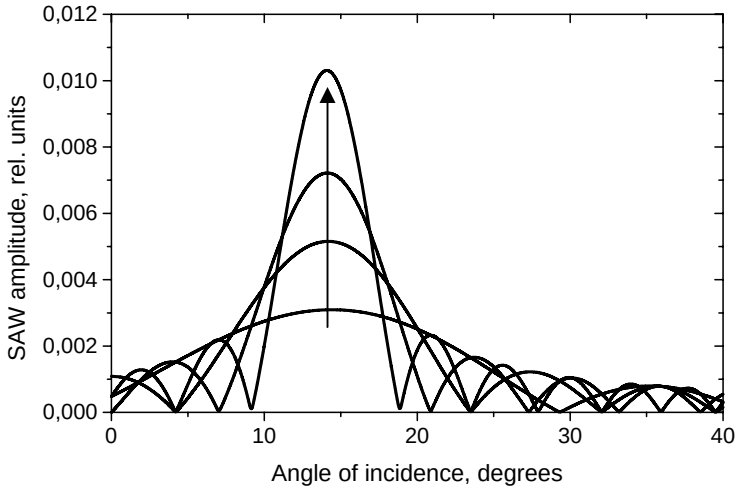

Figure 3. Calculated efficiency of ACU-SAW conversion in PMMA as a function of angle of incidence for different values of aperture (W) of 400-kHz-ACU-beam. The arrow corresponds to W = 3, 5, 7, and 10 mm.

3. Principle of operation

3.1 Slanted Transmission and Reflection Modes

The mode conversion in the slanted set-up enables to introduce an adjustable phase variation and to "stretch" the excitation along the surface. Under phase matching conditions, such a distributed source operates far more efficiently for the in-plane propagating waves, e.g. PAW, SAW or other types of interface waves.

To provide a high lateral resolution and thus local material probing with PAW excited in the slanted transmission, a configuration of focused ACU beams (Focused Slanted Transmission Mode (FSTM)) was developed [7]. It uses a pair of co-axial weakly-focused air-coupled transducers which face opposite sides of a specimen (Fig. 4 a).

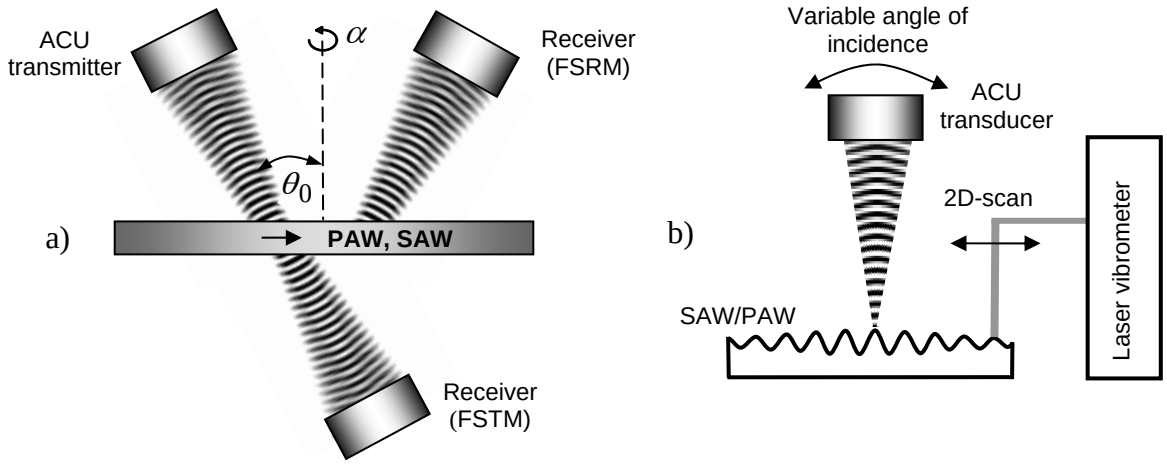

Figures 4 a, b. FSTM- and FSRM-configurations of ACU conversion (a); wave form imaging set-up (b).

In many applications, a single-sided access to a specimen is preferred that is provided in the non-contact pitch-catch configuration also shown in Fig. 4 a (Focused Slanted Reflection Mode (FSRM)). To suppress a specular reflection of the incident beam, the receiver is placed beside the transmitter with some sound absorbing material in between. Alternatively, in the pulse ACU-mode the time gate of the receiver is adjusted to select the PAW or SAW signal. As a result, unlike local probing in the FSTM, the FSRM-output is an average of the material properties over a certain distance (usually 3-5 cm).

3.2 Wavefront Imaging Mode (WIM)

The application area of ACU with mode conversion can be expanded substantially if the receiving transducer is capable of scanning the field of air-coupled plate or surface waves. Such a principle is realized in a fully non-contact configuration that comprises AC-excitation and acousto-optical (AO) laser scanning detection of the PAW and SAW field.

The scheme of the hybrid AC-AO-methodology is shown in Fig. 4 b. A weakly focused AC-transducer launches AC-ultrasonic waves on the front surface of the specimen. The variable angle of incidence θ ($0 - 90^0$) provides both cylindrical (at θ=0) and plane PAW/SAW excitation ($\theta = \theta_0$). The amplitude of the cylindrical wave radiated (along a certain direction) depends on the size of the aperture of the ACU beam. For a 2D-AC-surface source, a cylindrical wave is radiated whose waveform in the far-field region ($L > W^2 / \lambda$) is independent of the contour shape of the incident AC-beam and is determined by material properties only.

The wave field generated is scanned with a laser vibrometer responding to the out-of-plane component of vibration velocity. To analyse the total area of the specimen at θ=0, scanning is normally made over the rear surface of the plate; alternatively, a single sided AC-AO-access (Fig. 4 b) is used for an oblique AC-incidence. The output signal of the

vibrometer is compared with the reference voltage to result in recording of the phase synchronised time traces of vibration velocity. The data acquired are played back as a time sequence of 2D-frames, thereby displaying an animated picture of wave propagation.

4. Experimental Study of ACU-PAW/SAW Conversion

The experiments used commercial air-coupled equipment including weakly-focused (focus spot 3-4 mm) 390-450 kHz-piezo-ceramic transducers and a standard scanning table (ISEL-PRO-DIN). To measure the efficiency of mode conversion, the output signal in the FSTM/ FSRM configuration was compared with the amplitude of the ACU transmitted directly between the transmitter and receiver. For ACU-PAW conversion, the additional losses strongly depend on the value of θ_0 (Table 1). The data of the Table show that mode conversion provides a substantial enhancement in elastic coupling compared with conventional NTM. The gain obtained increases along with the values of θ_0, which indicates a contribution of space resonance. In fact, the length of the excitation area (in wavelengths) changes as $(W/\lambda_{air})tg\theta_0$ and rises sharply for large values of θ_0.

Table 1. Experimental results of ACU-PAW mode conversion (frequency 450 kHz).

Material	**Thickness (mm)**	θ_0 **(degrees)**	v_{a_0} **(m/s)**	**Conversion losses, dB (NTM)**	**Conversion losses, dB (FSTM)**	**Gain (NTM-FSTM)**
Paper I (A4)	0.1	52 ± 1	430 ± 10	44	20.5	23.5
Paper II	0.17	48 ± 1	460 ± 10	47	28.5	18.5
Al-foil	0.1	32 ± 1	640 ± 20	53.5	38.5	15
Polystyrene	1.1	21 ± 1	950 ± 50	64.5	53	11.5
Wood (spruce, L/LT)	0.65	19 ± 1	1040 ± 60	53	43	10

The measurements of ACU-SAW mode conversion were carried out in the FSRM configuration at 390 kHz and SAW propagation distance of ≈ 6 cm. Thus, a few *dB* of dissipation should be subtracted from some values of conversion losses given in Table 2. All values of θ_0 are smaller in this case, so that impact of the length of the excitation area is insignificant. Instead, a good correlation between conversion losses and the value of acoustic impedance of materials for SAW is observed. The only deviation in the case of concrete is apparently due to higher propagation losses in this material.

Table 2. Experimental results of ACU-SAW mode conversion.

Material	θ_0 **(degrees)**	v_{SAW} **(m/s)**	**Conversion losses, dB (FSRM)**	**SAW acoustic impedance (Mrayl)**
Fir (L/LT)	17 ± 0.5	1160 ± 30	37	0.9
PMMA	16 ± 0.5	1230 ± 40	40	1.5
Graphite	14 ± 0.5	1400 ± 50	45	2.1
Concrete	9 ± 0.5	2800 ± 200	61	5.3
Al	7 ± 0.5	2200 ± 100	54	7.8
Copper	10 ± 0.5	2000 ± 100	59	17.8
Steel	6.5 ± 0.5	3000 ± 200	63	23.4

5. NDT with Air-Coupled Mode Conversion

5.1 Defect Imaging in Slanted Modes

One of the advantages of using PAW and SAW for defect imaging is concerned with their strong damping due to scattering by material (and particularly subsurface) inhomogeneities. Besides the increase of acoustic scattering in the defect areas, an additional enhancement of contrast comes from the ACU conversion mechanism: a local variation of θ_0 causes a local drop in the generated (and received) wave amplitudes. The high sensitivity of the ACU-PAW in imaging of sub-surface defects is illustrated in Figure 5.

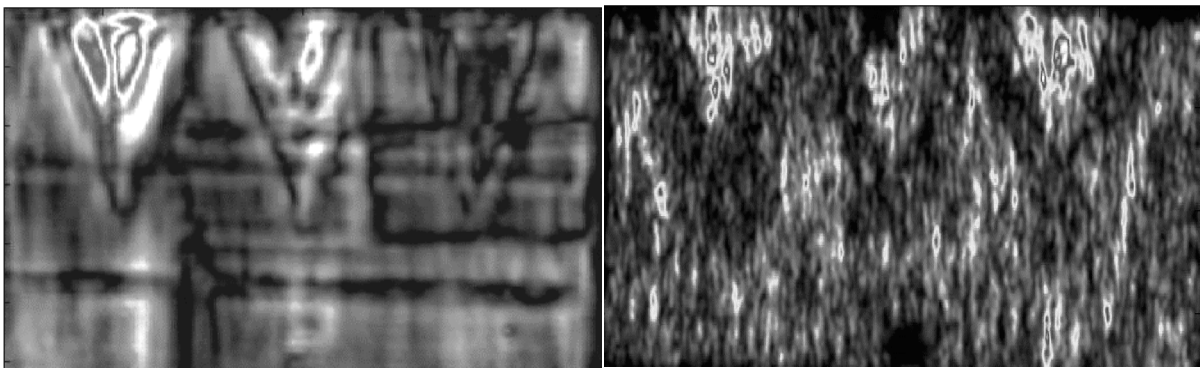

Figure 5. AC-plate wave imaging of simulated delaminations in honeycomb liners: front (left) and reverse (right) sides. Sample kindly provided by GROB Aerospace/Mindelheim-Mattsies.

The specimen measured is a honeycomb (thickness ≈ 5 cm) sandwitched between multi-ply carbon fiber-reinforced (CFR-) liners. To simulate delaminations, triangular shaped Teflon insertions were embedded between the honeycomb and the front side liner secured with glued CFR-repair patches. The structure of the laminate is clearly seen in the 390-kHz AC-PAW-image obtained in the FSRM (Fig. 5, left). The high sensitivity of PAW is emphasised in the image of the (intact) bottom side liner (Fig. 5 (right)). In this case, the AC-PAW visualizes the variation in strength of honeycomb-liner interface caused by the "imprints" of load applied while producing delaminations on the front side.

The angular dependence of ACU-PAW/SAW conversion makes possible a selective excitation of PAW or SAW which could be applied for NDT of hidden cavities. Figure 6 (right) shows a 2-cm thick Al-sample (30x20 cm) with three cavities of different depths. The thickness of residual material in the cavity areas varies from 1 to 3 mm. The results

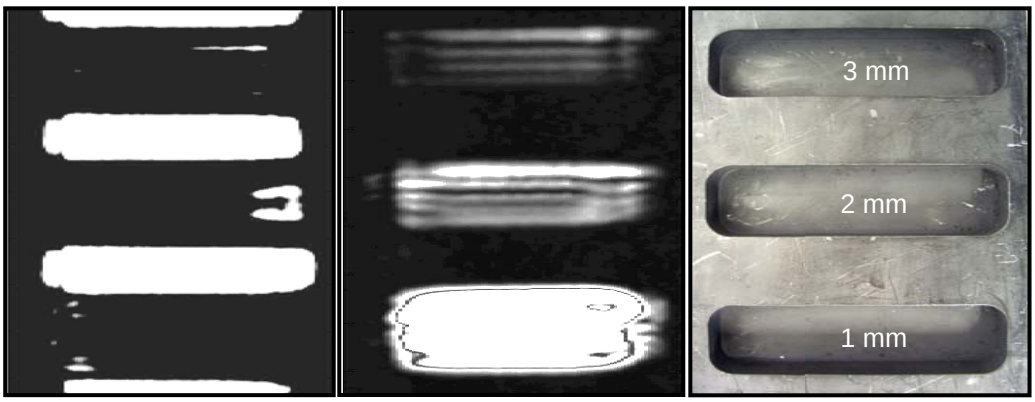

Figure 6. Single-sided scans of hidden cavities in Al-sample (right): AC-SAW (left) and AC-PAW (middle).

of single-sided scanning (over intact side) at the resonant angle for ACU excitation of PAW in the 1-mm thick area (middle) reveal the cavities and indicate the difference in their depths. The SAW scan (left) exhibits a mirror-inverse contrast with higher output in parts of regular thickness while the cavities are displayed as low-contrast areas.

5.2 NDT of Films and Coatings

Since PAW and SAW in layered structures exhibit substantial dispersion, both amplitude and phase of the FSTM- and FSRM- output signals are sensitive to variation of thickness and can be used for a remote thickness profilometry of films and coatings. An example of the FSTM-B-scanning of inhomogeneous thickness of paint is given in Figure 7. One can see that variation of the delay (phase) of the output signal (right) basically follows the coating profile. The high phase sensitivity of the FSTM-output to deviation in paint thickness ($\approx 4^0$ /μm, Figure 7) confirms the feasibility of high-accuracy profilometry of paint coatings on steel substrates typical for automotive industry.

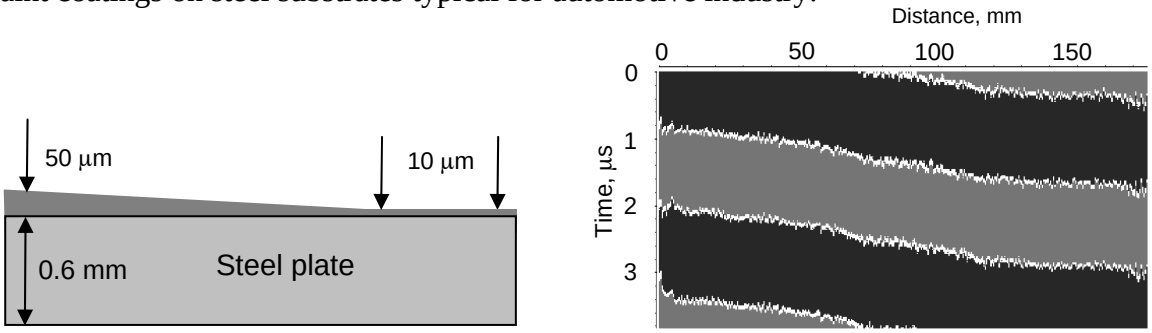

Figure 7. FSTM-profilometry: (left) configuration of paint coating; (right) FSTM-B-scan (white lines indicate positions of zero displacements).

The SAW/PAW velocity and dissipation also depend on stiffness and viscosity of coatings. As a result, the FSTM- and FSRM- output signals are sensitive to changes in the physical state of films and coatings (hardening, polymerization, drying, etc.). Both amplitude and phase of AC-SAW/PAW can be used for real time non-contact monitoring of such processes on-site in an industrial environment. An example of application of AC-SAW for monitoring of drying of paint is illustrated in Figure 8. It shows that drying of identical paints develops differently for concrete and PMMA substrates. In the concrete, the reaction proceeds more intensively (higher values of phase derivative) and faster (drying time ~ 4500 s against ~ 8000 s in PMMA) because the paint solvent is inactive for concrete.

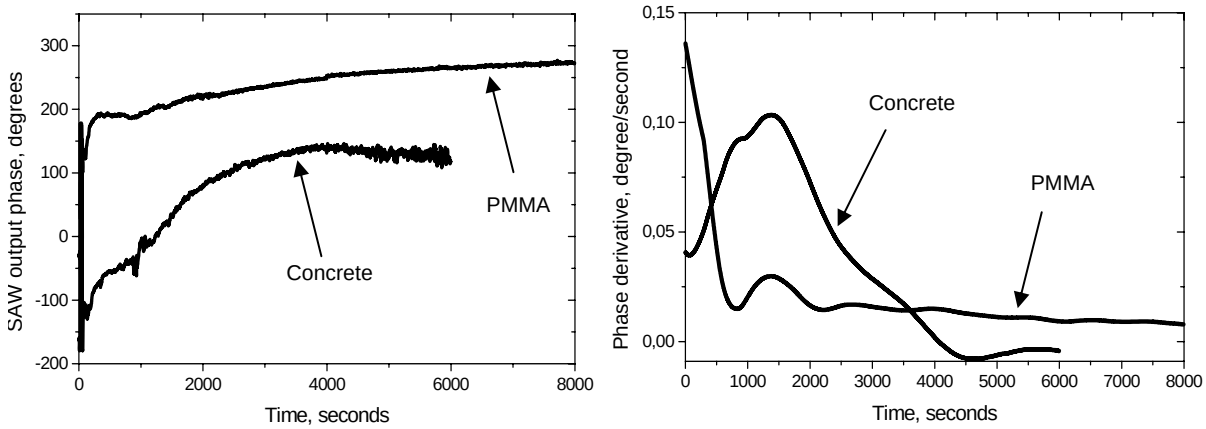

Figure 8. AC-SAW monitoring of drying paint: output phase (left) and its derivative (right) variations in time.

5.3 Material Inspection in Wavefront Imaging Mode (WIM)

Unlike the case of bulk acoustic waves which are confined in the interior of a solid, a surface access to PAW/SAW field makes them particularly attractive for direct visualisation of defects and imperfections in materials. The wave-defect interaction causes both amplitude and phase distortions of the guided wave field, therefore WIM permits remote discerning of a wide range of flaws.

An example of the WIM application for visualization of defects is shown in Figure 9 (left) for AC-PAW propagating along fibers in a unidirectional CFR-composite with impact damage. The wave amplitude perturbation is caused by wave scattering at cracked fiber fragments and localised exclusively inside the damaged area.

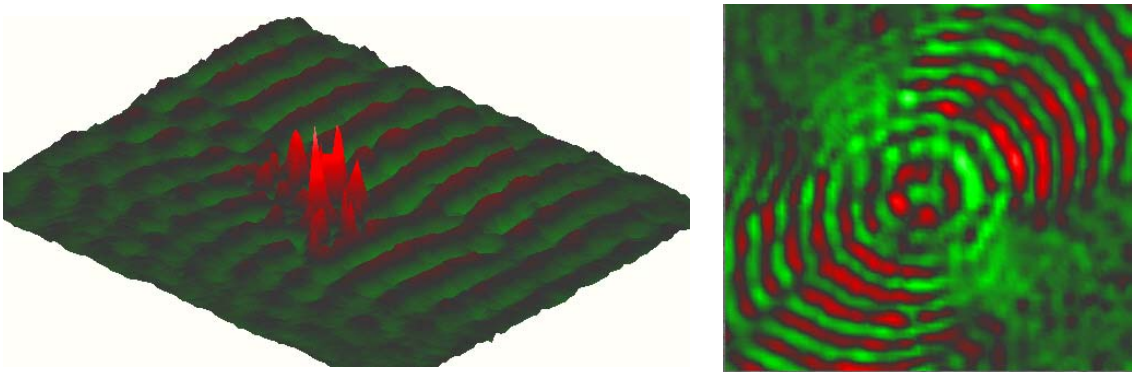

Figure 9. Material inspection in WIM: AC-PAW scattering by an impact in CFR-composite (left); anisotropy of PAW propagation in beech veneer (right).

As was mentioned in Section 3.2, at $\theta_0 = 0$, the focused ACU is converted into a cylindrical PAW/SAW whose wavefront is independent of the source geometry and thus is formed by the in-plane stiffness anisotropy of the material. The latter is an important parameter which determines mechanical performance of engineering components made from composite materials. The feasibility of imaging of stiffness anisotropy by using the WIM is demonstrated in Figure 9 (right). An obvious elongation of the wavefront in the 45^0-direction indicates the fiber orientation in the material. By measuring of the wavelengths along and across the fibers in Fig. 9, the values of PAW velocities are found to be $\approx$ 1000 m/s and $\approx$ 660 m/s, respectively, that quantifies asymmetry of the in-plane stiffness anisotropy in the material tested. Thus, application of the WIM can provide a method for a rapid interrogation of material elastic anisotropy and, in particular, its uniformity over large areas.

References

[1]. A.J. Rogovsky, Development and application of ultrasonic dry-contact and air-contact C-scan systems for non-destructive evaluation of aerospace components, Material Evaluation, 50, 1491-1497, 1991.

[2]. J. Krautkrämer and H. Krautkrämer, *Ultrasonic Testing of Materials*, Springer-Verlag, Berlin, 1990.

[3]. A. Briggs. *Acoustic Microscopy*, Clarendon Press: Oxford, 1992.

[4]. L.M. Brekhovskikh, *Waves in Layered Media*, Academic Press, New York, 1960.

[5]. I.A. Victorov. *Rayleigh and Lamb Waves*, Plenum Press, N[ew York (1967).

[6]. I. Solodov, K. Pfleiderer, and G. Busse, Laser vibrometry of air-coupled Lamb waves: a novel methodology for non-contact material characterization, Materialprüfung, 47, 3, pp. 3-7, 2005.

[7]. I. Yu. Solodov, R. Stoessel, G. Busse, Material characterization and NDE using focused slanted transmission mode of air-coupled ultrasound, Research in Non-Destructive Evaluation, v.15, pp. 1-21, 2004.